Influence of mesostructuration on the reactivity of bioactive glasses in biological medium: a PIXE-RBS study†

J. Soulié,[abc] J. Lao,[a] E. Jallot[a] and J. M. Nedelec*[bc]

DOI: 10.1039/c2jm30880k

Building mesostructured biomaterials is a challenging and exciting task that has attracted much attention because of their use as drug carriers or drug delivery systems. In the case of bioactive materials, the mesostructuration can also deeply impact their physico-chemical properties and the reactivity. In this study, we show how highly ordered mesoporosity influences the early steps of the biomineralization process and the reactivity in binary (SiO_2–CaO) and ternary (SiO_2–CaO–P_2O_5) bioactive glasses. Conventional porous sol–gel glasses were synthesized using a classical route, while mesostructured glasses were developed using a non-ionic surfactant. Textural properties of these materials have been characterized. The *in vitro* biomineralization process was followed, using Particle Induced X-ray Emission (PIXE) associated to Rutherford Backscattering Spectrometry (RBS), which are efficient methods for a highly sensitive multi-elemental analysis. Elemental maps of silicon, calcium and phosphorus were obtained at a micrometer scale and revealed for the first time a bulk reactivity for mesostructured glasses. This is a major advantage over conventional glasses, for which the first steps of biomineralization are limited to the periphery of the material. Their enhanced bioactivity combined with their possible use as drug-delivery systems make them promising candidates for bone regeneration.

1. Introduction

Highly ordered mesoporous materials have been widely studied as drug delivery systems during the past decade (antitumorals,[1] antibiotics,[2] anti-inflammatory[3]). In the case of bone reconstruction, implantation of such systems has several advantages over conventional materials. Indeed, the main interest of these materials is the control of kinetics and the spatiality of molecules release, which implies a higher efficiency of delivery, a reduced toxicity, and a continuous action. Several kinds of materials like mesoporous carbons, bioceramics or polymers have been studied, but the most described drug delivery system is silica.

For bone regeneration, an attractive solution is the synthesis of mesostructured bioactive glasses *via* sol–gel routes. When implanted, these materials are able to bond to living bones through the formation of an interfacial apatite-like layer at the glass surface, the composition of which is close to the mineral phase of bones.[4] This newly formed biomimetic layer improves the osteo-integration properties of the implant, while the degradation products from the glass promote the bone tissue regeneration. Synthesis of binary (SiO_2–CaO), ternary (SiO_2–CaO–P_2O_5) or even doped mesostructured bioactive glasses has been described in some publications.[5–7] Their *in vitro* drug release behaviors have also been evaluated.[8] Moreover several research groups investigated the influence of the mesostructuration on physico-chemical reactions (dissolution, diffusion, ionic exchange and precipitation).[9–11] These studies demonstrated that the increase of the specific surface area (higher silanol concentration[12]) and pore volume of bioactive glasses has an effect on the kinetics of reaction and on the structural evolution of the calcium phosphate phases formed at the glass interface. The present study aspires to add spatial information about the physico-chemical reactions occurring when bioactive glasses are in contact with biological media. Differences between conventional porous sol–gel glasses and mesostructured glasses will be explained using Particle Induced X-ray Emission coupled to Rutherford Backscattering Spectrometry (PIXE-RBS). These nuclear techniques allow monitoring the spatial distribution and diffusion of elements within bioactive glasses with an excellent (a few ppm) sensitivity, through the recording of quantitative chemical maps of glass grains after interaction with biological fluids.

[a]*Clermont Université, Université Blaise Pascal, CNRS/IN2P3, Laboratoire de Physique Corpusculaire, BP 10448, 63000 Clermont-Ferrand, France*
[b]*Clermont Université, ENSCCF, Institut de Chimie de Clermont-Ferrand, BP 10448, 63000 Clermont-Ferrand, France. E-mail: j-marie.nedelec@ensccf.fr; j-marie.nedelec@univ-bpclermont.fr; Tel: +33 4 73 40 71 95*
[c]*CNRS, UMR 6296, ICCF, 63171 Aubière, France*

2. Materials and method

2.1. Synthesis

Binary (SiO_2–CaO) and ternary (SiO_2–CaO–P_2O_5) mesostructured glasses have been synthesized through a sol–gel route, by using a commercially available nonionic surfactant Pluronic F127 (BASF) as a structure-directing agent. These materials are labeled B75-F127 and B67.5-F127 depending on their chemical composition (Table 1). Tetraethylorthosilicate ($Si(OC_2H_5)_4$) TEOS, triethylphosphate ($PO(OC_2H_5)_3$) TEP, and calcium nitrate tetrahydrate ($Ca(NO_3)_2 \cdot 4H_2O$) CaNT (Aldrich) were used as SiO_2, CaO and P_2O_5 sources. The amounts of reactants are indicated in Table 1.

In a typical synthesis of mesostructured glasses (MG), F127 is dissolved in ethanol (18 mL). At the same time, stock solution is prepared by mixing TEOS, TEP, CaNT, H_2O, HCl (2 M) and EtOH. After stirring them separately for 1 h, both solutions are mixed and vigorously stirred together for another 4 h. The resulting sol is introduced into a Petri dish to undergo an Evaporation-Induced Self-Assembly (EISA) process[13] for 48 h. The dried gel is then calcined at 600 °C for 12 h to eliminate the surfactant and to obtain the final glass powder. The complete elimination of the surfactant was checked with FTIR spectroscopy. For comparison, conventional porous glasses (CG), named B75 and B67.5 and with the same compositions (Table 1), have also been synthesized by a similar sol–gel process but without surfactants.

2.2. Materials characterization

Nitrogen gas sorption analyses were performed to characterize the textural properties of glasses. The samples were vacuum outgassed at 120 °C for 12 hours to remove physically adsorbed molecules from the pores. The adsorption–desorption isotherms were recorded on a Quantachrome Autosorb-1 MP apparatus. The instrument determined isotherms volumetrically by a discontinuous static method at 77 K. The surface areas were obtained by applying the BET method to the N_2 isotherm using 7 points in the 0.05–0.35 p/p_0 range. The pore size distribution was determined by applying the BJH method on the desorption branch. Total pore volume was measured at a relative pressure $P/P_0 = 0.995$. The average pore diameter was calculated using surface area and total pore volume and considering cylindrical pores.

Powder X-ray diffraction experiments were performed with an X'Pert Pro diffractometer equipped with Cu Kα radiation (wavelength 1.5406 Å). XRD patterns were collected in the 2Θ range between 0.6° and 3.1° with a step size of 0.02° and a counting time of 5 s per step.

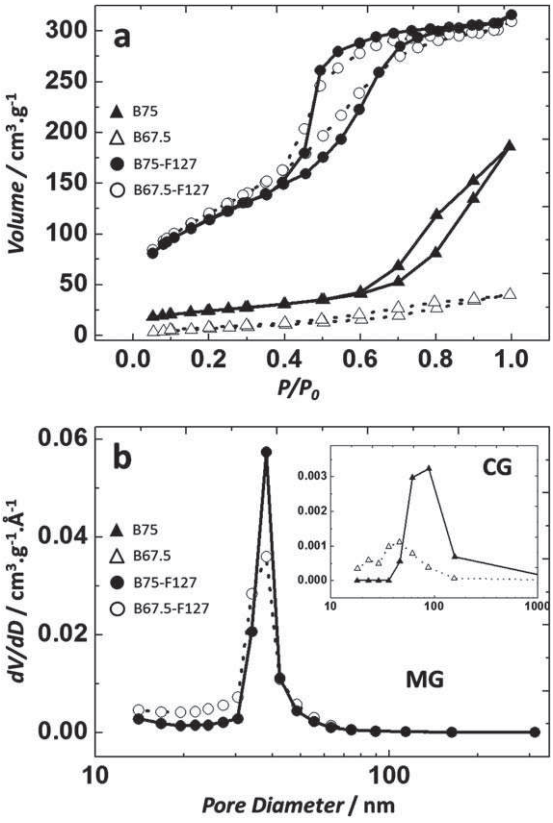

Fig. 1 Nitrogen adsorption–desorption isotherm plots (a) and pore size distribution curves (b) of calcined glasses: B75-F127(○), B67.5-F127(●), B75 (△), and B67.5(▲).

Transmission electron microscopy (TEM) was carried out with a Hitachi H-7650 microscope, operating at 120 kV (resolution 2Å). Images were recorded using a CCD camera (Hamamatsu HR, 1024 × 1024 pixels).

2.3. *In vitro* studies and samples preparation

For studying the glass reactivity under biological conditions, glass powders were immersed at 37 °C for 15 minutes, 30 minutes, 1 hour, 6 hours, 12 hours, 1 day, and 2 days in 40 mL of a standard Dulbecco's Modified Eagle Medium (DMEM, Biochrom AG, Germany) in which concentrations of inorganic salts are close to those of human plasma.[14] Mandel and Tas[15] demonstrated that DMEM can be regarded as a feasible alternative to using Simulated Body Fluid (SBF) solutions for *in vitro* bioactivity testing of synthetic biomaterials. Unlike SBF, DMEM contains amino acids, vitamins and glucose. Because of amino acids, lower rates for the materials dissolution and a

Table 1 Nominal compositions and amounts of reactants for the synthesis of mesostructured and conventional sol–gel B75 and B67.5 glasses

Sample	Nominal composition (wt%)	TEOS (g)	CaNT (g)	TEP (g)	HCl (2 M) (g)	H_2O (g)	EtOH (total amount, g)	F127 concentration (wt%)
B75-F127	75 SiO_2–25 CaO	6.47	2.63	0	1	3.15	19.73	7.95
B67.5-F127	67.5 SiO_2–25 CaO–7.5 P_2O_5	5.82	2.63	0.48	1	3.08	19.73	7.88
B75	75 SiO_2–25 CaO	6.47	2.63	0	1	3.15	7.89	0
B67.5	67.5 SiO_2–25 CaO–7.5 P_2O_5	5.82	2.63	0.48	1	3.08	7.89	0

subsequent delay in surface layer formation are observed in DMEM when compared to soaking in SBF.[16] Indeed amino acids from DMEM are charged species that can be attracted by the negative glass surface and form a film at its surface. In terms of simulating the *in vivo* environment, DMEM can be a better choice as it also contains other components present in *in vivo* systems besides inorganic salts.[14] For the same reasons, DMEM is commonly used in cell culture,[17–19] contrary to SBF (because of its deficiency of nutrients[20]). Hence we decided to use DMEM in the present study for further comparison with biological results.

To simulate homeostasis of a real biological system, interactions under dynamic conditions are better adapted. Indeed, it has been demonstrated[21] that results of dynamic and static procedures differ for several parameters (constant concentration of interesting elements, constant pH…), and that the dynamic procedure is closer to *in vivo* conditions. Despite these advantages, the static procedure has been classically chosen in this work because of its easier implementation. Moreover, its use allows also direct comparison of the different mesostructured glasses with samples described previously in the literature for which static conditions were mainly used.

For each sample, the powder weight to DMEM volume ratio was fixed to allow studying the influence of the textural effects only, on physico-chemical properties. After interaction, part of the DMEM was sampled to analyze its chemical composition by Inductively Coupled Plasma-Atomic Emission Spectroscopy (ICP-AES), while the glass particles were removed from the solution and air dried. Before characterization with a PIXE-RBS nuclear microprobe, glass particles were embedded in the resin (AGAR, Essex, England). 1000 nm thin sections of these samples were prepared by means of a Leica EM UC6 Ultramicrotome, and inserted in 50 mesh copper folding grids, which were placed on a Mylar film with a hole of 3 mm in the centre. Measurements were performed on the area of the section placed over the hole.

2.4. PIXE-RBS analysis

PIXE and RBS methods are used simultaneously. The PIXE method permits the identification and the quantification of elements in sections of biomaterial grains after interaction with biological medium.[22] RBS is used to determine the electric charge received by the samples during irradiation, which is necessary for PIXE spectra quantification. Analyses of our materials were carried out using nuclear microprobes at the CENBG (Centre d'Études Nucléaires de Bordeaux-Gradignan, France). The experimental characteristics of the CENBG microbeam line have been published previously.[23,24] For PIXE-RBS analyses, we chose a proton scanning microbeam of 1.5 MeV energy and 50 pA in intensity. The beam size was nearly 1 μm. Such parameters resulted in higher ionization cross-sections for light elements ($Z < 20$) and thus in a better sensitivity for PIXE analysis by using a detector without filter. Furthermore, weak intensities and the choice of protons as the ion beam allowed the target degradation to be minimized during irradiation. However, the intensities were sufficient to permit measurement duration below 1 h. An 80 mm^2 Si(Li) detector was used for X-ray detection, orientated at 135° with respect to the incident beam axis, and equipped with a 12 μm thick beryllium window. PIXE spectra were treated with the software package GUPIXWin. For RBS measurements, a silicon particle detector placed at 135° from the incident beam axis provided us with the number of protons that interacted with the sample. Data were treated with the simNRA code.

3. Results

3.1. Textural properties

Fig. 1a shows the N_2 sorption isotherms for the mesostructured glasses (MG) and conventional sol–gel glasses (CG). Contrary to CG, MG curves can be identified as type IV isotherms characteristic of porous materials. B75-F127 and B67.5-F127 show type H1 hysteresis loops in the mesopore range, which are characteristic of cylindrical pores open at both ends. The pore size distributions are shown in Fig. 1b. MG present a single-modal pore size distribution centered around 4 nm, whereas CG pore size distributions are not very well defined and exhibit much bigger pore sizes. Table 2 collects the specific surface area, mesopore volume, and pore size measured for the four samples. Specific surface areas are significantly higher for the mesostructured glasses than those obtained for conventional sol–gel glasses of analogous compositions (from 4× up to 15×). This increase is essentially due to the specific surface area associated to the mesoporosity. In the same way, pore volume is also higher for MG compared to that in CG. The modal pore diameter and average pore diameter are close for the two mesostructured materials, which confirm the hypothesis of cylindrical pores and consequently the successful templating.

Fig. 2 presents the images of Transmission Electron Microscopy (TEM) of B75-F127 and B67.5-F127 glasses. After calcination, organized networks of mesopores are present for both materials. The observed hexagonal structure is confirmed in other articles[25,26] for similar syntheses in the same domains of the ternary diagram H_2O/EtOH/F127. The results of X-ray diffraction at small angles abound in this direction, as the identified peaks ($h = 1, k = 0$) and ($h = 1, k = 1$) (Fig. 3) are consistent with

Table 2 Textural properties of conventional sol–gel and mesostructured B75 and B67.5 glasses

	B75	B67.5	B75-F127	B67.5-F127
BET surface area ($m^2\ g^{-1}$)	30	112	442	410
BJH modal pore diameter (nm)	4.6	8.9	4.3	3.9
Average pore diameter (nm)	8.4	13.2	4.3	4.8
Total pore volume ($cm^3\ g^{-1}$)	0.062	0.289	0.444	0.490

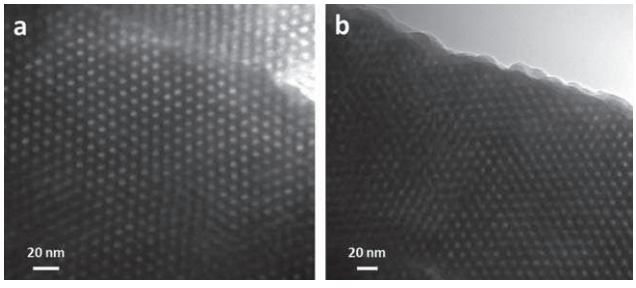

Fig. 2 TEM images for mesostructured glasses: B75-F127 (a) and B67.5-F127 (b).

a *P6mm* hexagonal symmetry of cylindrical pores. These peaks, whose positions are given in Table 3, permitted calculation of the lattice parameters using Bragg's law. These parameters are close for both glasses. Distances estimated using average measurements on TEM images confirm a similar order of magnitude.

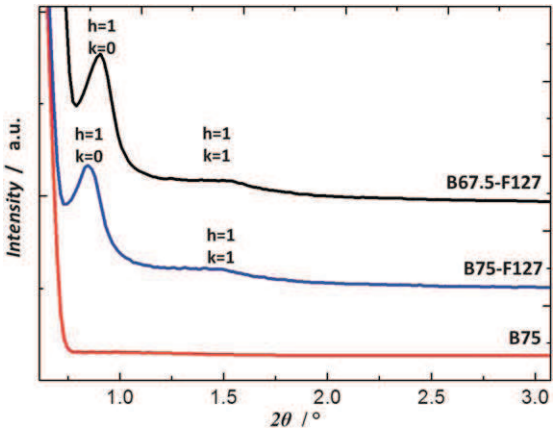

Fig. 3 Small Angle XRD patterns for B75, B75-F127 and B76.5-F127 glasses.

Table 3 Lattice parameters and wall thickness measured by XRD and TEM

	XRD			TEM	XRD/BET
	2θ (°)				
	$h = 1$, $k = 0$	$h = 1$, $k = 1$	a (nm)	a (nm)	Wall thickness (nm)
B75-F127	0.84	1.49	12.12	11.2	7.8
B67.5-F127	0.9	1.6	11	9.8	7.1

3.2. Elemental mapping

Several elemental maps for each time of interaction with DMEM were recorded. In this paper, we only present a restricted selection of these maps. The observed distributions correspond to the intensity of X-rays locally emitted by the sample under proton irradiation.

Fig. 4 shows evolutions of chemical mapping for binary glasses. Before immersion in DMEM (0 day), elemental distributions of silicon and calcium are homogeneous in the grains of both B75 and B75-F127. After 1 h of immersion distributions evolve in two different ways. For B75 glass, a layer is formed at the periphery. This layer is rich in calcium and phosphorus. At the same time, a loss of calcium is observed in the inner region. For longer interaction time (2 days) the phosphocalcic layer disappears and only silica remains as discussed in previous work.[27] For B75-F127 glass, distributions and concentrations of calcium seem stable compared to the material before interaction. Phosphorus from the biological medium is integrated in the volume of the grain and not only at the periphery as for B75. After 2 days of interaction, a persistence of silica matrix is observed for the two glasses. However, unlike the B75 glass, calcium and phosphorus are still present within the mesostructured material intimately mixed with silicon oxide.

Ternary glasses (Fig. 5) maintain a homogeneous elemental distribution from 0 day to 1 hour for CG and MG. However behaviors of both materials differ thereafter. Indeed after 2 days, the core/layer spatial discrimination observed for B67.5 is not applicable for B67.5-F127. The mesostructured glass is then mainly composed of calcium and phosphorus and the silicon concentration seems very low.

For both materials, the main trend highlighted by the chemical mapping is the spatial discrimination of elemental distribution observed for conventional sol–gel glasses (formation of a phosphocalcic layer at the periphery) and not for mesostructured glasses.

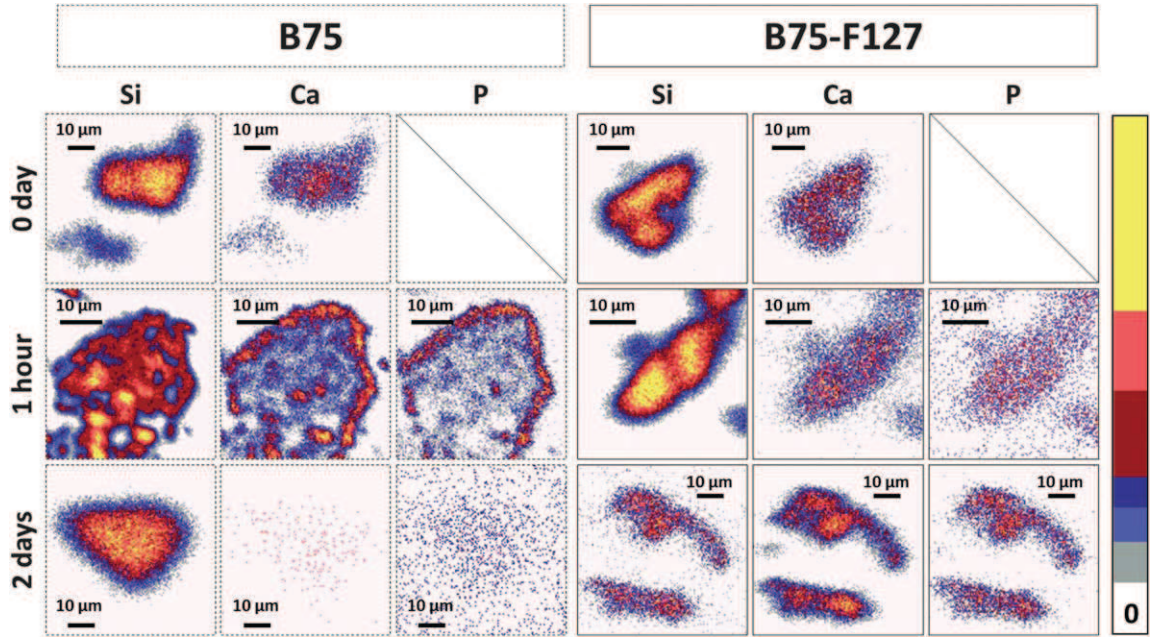

Fig. 4 Representative elemental maps of grains of binary glasses before interaction and after 1 hour and 2 days of interaction with biological fluids.

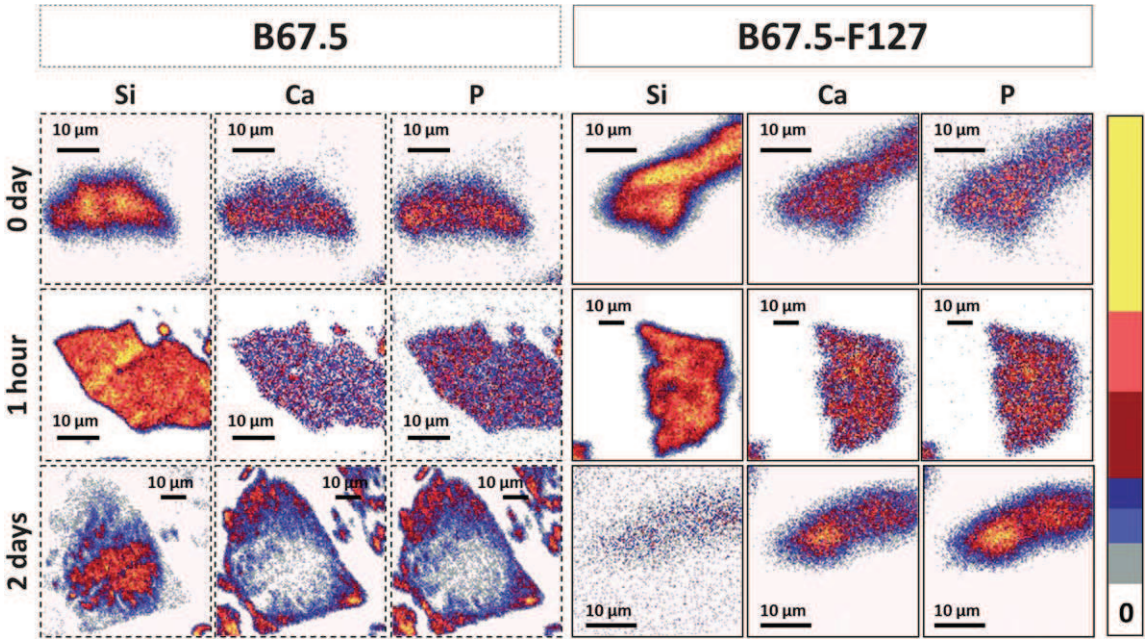

Fig. 5 Representative elemental maps of grains of binary glasses before interaction and after 1 hour and 2 days of interaction with biological fluids.

3.3. Evolution of the concentrations in the grains

The PIXE-chemical maps were divided into various regions of interest using the SUPAVISIO analysis software. Whenever the Ca–P-rich layers were detected, areas of measurement were created at the periphery and in the inner region of grains, focusing on the X-ray spectra of these user-defined regions of interest. Even if layers are not observed for mesostructured glasses, the same methodology has been used. Then elemental concentrations were calculated in these areas and thanks to the elemental concentrations measured for each delay, the temporal evolution of concentrations for each region can be monitored. The results correspond to the average concentrations calculated in several identical regions of interest. These regions of interest were defined for various samples in order to ensure reproducibility of measurements. Each point represents an average of 5 measurements.

Errors in elemental concentrations are associated to the statistical uncertainty due to the differences of concentrations for all the measurements used to obtain the average. The uncertainty associated to each point is then calculated thanks to an empirical standard deviation. These errors, which are not represented on the graphs for a better reading, are below 5% for Si, 10% for Ca and 7% for P. Taking into account the uncertainties, general and reliable trends can still be observed.

Evolutions of concentrations at the periphery and in the inner region of mesostructured grains are the same. Consequently B75-F127 and B67.5-F127 curves represent global evolution of the grains.

Binary glasses. The overall concentrations evolution of mesostructured glass is compared to peripheral (Fig. 6) and internal (Fig. 7) evolutions of conventional sol–gel glass. The evolution at the interface of B75 glass (Fig. 6) is in agreement with mechanisms described for this kind of glass.[28] First there is the formation of a Ca–P layer between 1 hour and 6 hours. Indeed, during this period a significant increase in concentrations of calcium and phosphorus is observed. This phenomenon is logically associated with a decrease of silicon. Subsequently, this layer dissolves from 6 hours to 2 days (loss of calcium and phosphorus and predominance of silicon). The core of the B75 glass (Fig. 7) undergoes a release of Ca^{2+} and despite the incorporation of phosphorus (between 0 and 1 day), its main component is silicon.

In the case of the mesostructured glass, the decrease of calcium before 1 hour (opposite effect of silicon) is due to the

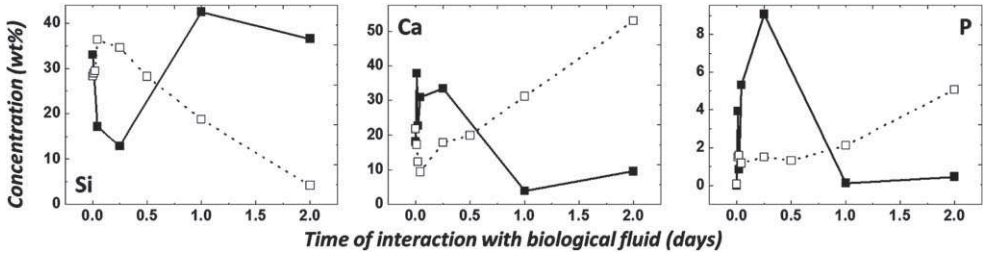

Fig. 6 Evolution of elemental concentrations at the periphery of B75 grains (■) and in the volume of B75-F127 grains (□).

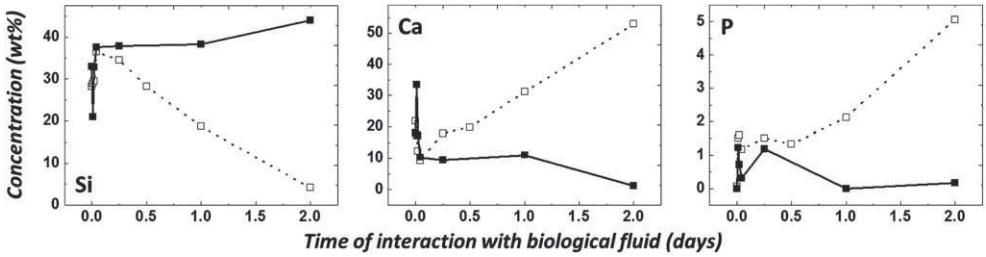

Fig. 7 Evolution of elemental concentrations in the inner region of B75 grains (■) and in the volume of B75-F127 grains (□).

dealkalinization of the material. The evolution of this process over the time is close to the one at the center of the grain of glass B75 (Ca and P evolutions, Fig. 7). Moreover, while calcium phosphate is only formed on the surface of the B75 glass, it is present within the total volume of B75-F127 grains, as demonstrated by consistent increases in Ca and P (Fig. 7). This calcium phosphate also appears more stable or still in formation, because it does not dissolve, in contrast to the phosphate layer of conventional sol–gel glass (low Ca and P between 6 hours and 2 days). The last remark concerns the important decrease of the silicon concentration for the mesostructured material, whereas that of the B75core remains relatively stable. This phenomenon does not automatically mean increased dissolution of the silica network, but may reflect a decrease in its mass contribution to the benefit of the phosphate phase.

Ternary glasses. As for binary glasses, the global evolution of the mesostructured material is compared with that of the conventional sol–gel material. Curves corresponding to the elemental evolution in the total volume of B67.5-F127 and to the evolution at the periphery of B67.5 glass are presented in Fig. 8. The first important point is the similarity of the two curves for each of the three elements. In both cases the decrease of calcium concentration (and respectively the increase of silicon concentration), reflecting the network dealkalinization, takes place between 0 and 1 hour. Subsequently, the concomitant increases in calcium and phosphorus can be interpreted by the formation of calcium phosphate precipitates within the grain for the mesostructured glass and at the periphery for the conventional sol–gel glass. Given these results, it is clear that mechanisms occurring in the two cases are similar (kinetics, intensity). Consequently the mesostructured glass allows not only a surface, but a three-dimensional formation of a phosphocalcic phase.

3.4. Elemental evolution of the biological medium

Binary glasses. The evolutions of silicon, calcium and phosphorus concentrations in the biological medium (Fig. 9) confirm some trends outlined by local measurements in grains of B75 and B75-F127 glasses. First, variations of calcium concentrations between 0 and 1 hour support the theory of very similar kinetics of dealkalinization for both materials. After reaching a maximum, the calcium concentration decreases much faster for the B75 glass than for the B75-F127 glass between 1 hour and 2 days. The amplitude and the kinetics of the phosphorus decrease are also higher for the conventional sol–gel glass. The curves

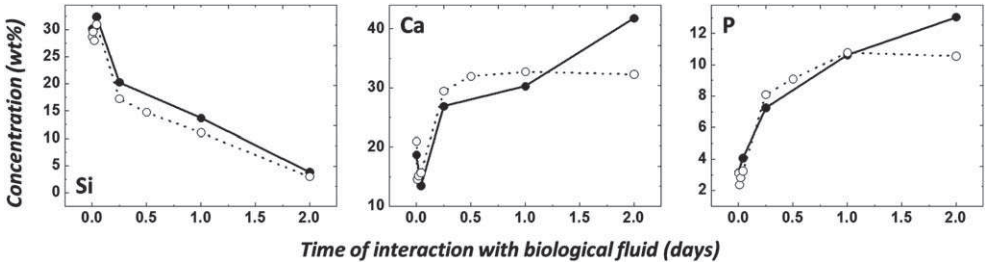

Fig. 8 Evolution of elemental concentrations at the periphery of B67.5 grains (●) and in the volume of B67.5-F127 grains (○).

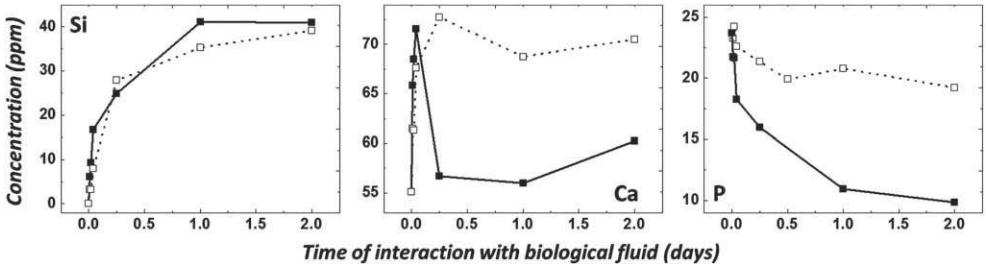

Fig. 9 Evolution of elemental concentrations in biological fluids for B75 (■) and B75-F127 (□) glasses.

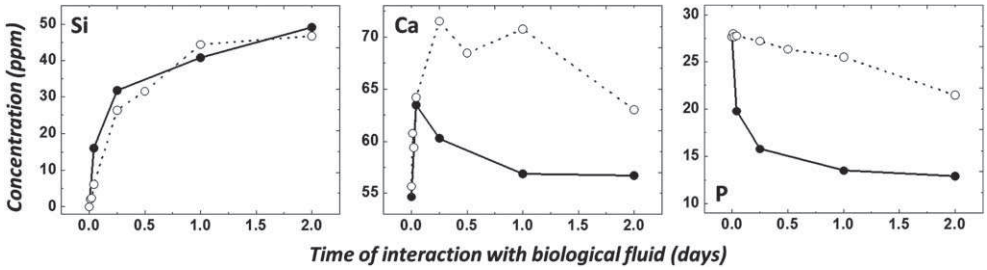

Fig. 10 Evolution of elemental concentrations in biological fluids for B67.5 (●) and B67.5-F127 (○) glasses.

representing silicon, for which evolutions are almost the same for B75 and B75-F127, invalidate the hypothesis of a larger dissolution of the glassy matrix for the B75-F127 glass.

Ternary glasses. The concentration changes of DMEM during interaction with B67.5 and B67.5-F127 glasses are presented in Fig. 10. Similarly to the binary glass, the same trends of silicon evolution indicate that the kinetics and intensity of the degradation of the silica matrix are very similar for both glasses. The kinetics of calcium release are also very close (maximum between 0 and 1 h for B67.5 and between 0 and 6 h for B67.5-F127), although the amount of released calcium into the biological medium is more important for the mesostructured glass. This difference may potentially be explained by reactivity within the volume for B67.5-F127. Finally, as for the binary glass, the decrease in phosphorus concentration is much less important for the mesostructured glass.

4. Discussion

Changes in elemental concentrations are powerful indications on how mesostructured glasses react in an acellular medium. The specific surface area is considerably increased from conventional sol–gel glasses to mesostructured glasses (from 4× for ternary glasses to 15× for binary glasses), thanks to homogeneous and interconnected nanoscaled porosity. This large specific surface area allows a three-dimensional homogeneous reactivity for dealkalinization, dissolution of the silicate network and biomineralization.

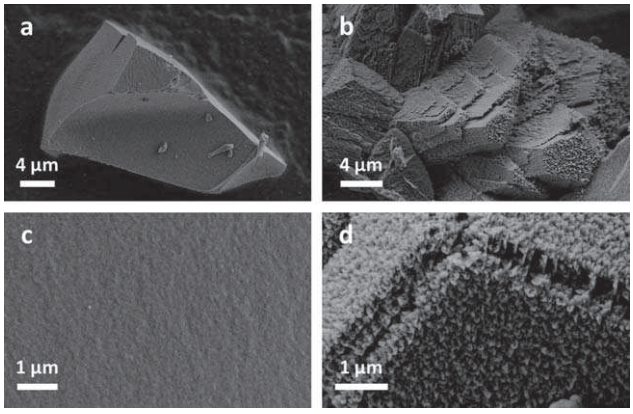

Fig. 11 SEM images of B75-F127 glass before (a and c) and after 12 hours (b and d) of immersion in DMEM.

4.1. Compositional evolution of phosphocalcic phases

Ca–P phases formed at the beginning of the biomineralization process are partially crystallized and embedded in amorphous silica, which makes XRD unusable to follow structural changes. NMR or vibrational spectroscopies, which are powerful techniques to understand structural evolutions, could be helpful but they are either global (NMR, FTIR) or surface sensitive (Raman) techniques. Although PIXE-RBS does not directly probe the phase structure, it allows addition of complementary information about the three-dimensional evolution of phosphocalcic phases nature, thanks to the evolution of Ca/P atomic ratio over time.

Fig. 11 presents SEM images of a B75-F127 glass before and after 12 hours of immersion in the biological medium. These pictures clearly show that new phases have been formed during the interaction. According to elemental maps obtained with PIXE, these phases are calcium phosphates. Three phosphocalcic phases are mainly formed in biological fluids such as SBF or DMEM:[29] dicalcium phosphate and octacalcium phosphate which are metastable phases and hydroxyapatite which is the most thermodynamically stable phase and therefore the less soluble (Table 4).

The nature of the phase was monitored *via* the Ca/P atomic ratio measured at the glass–biological medium interface for conventional sol–gel materials and within the grain for mesostructured materials. Curves representing these evolutions as a function of interaction time are shown in Fig. 12 for binary and ternary glasses.

For the binary glasses, the Ca/P ratio reaches a minimum value for both materials after 1 hour of interaction. However these minima differ on several points: the minimum is lower (2.85 *versus* 5.7) for the B75 glass. It is also reached in a shorter time for the B75 sample and is already close to 23 after 6 hours because of the dissolution of the layer. This quite low ratio and the dissolution of the phase indicate the formation of metastable phases mentioned above. Although they are less stable than apatite, precipitation kinetics of these phases is faster.[29] For the

Table 4 Main Ca–P crystalline phases formed in SBF or DMEM

Name	Formula	Ca/P atomic ratio
Dicalcium phosphate	$CaHPO_4 \cdot 2H_2O$	1
Octacalcium phosphate	$Ca_8(HPO_4)_2(PO_4)_4 \cdot 5H_2O$	1.33
Hydroxyapatite	$Ca_{10}(OH)_2(PO_4)_6$	1.67

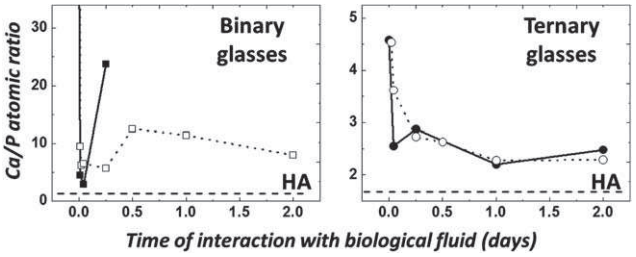

Fig. 12 Evolution of Ca/P atomic ratio for B75 (■), B75-F127 (□), B67.5 (●) and B67.5-F127 (○) glasses.

conventional B75 glass, the surface reactivity (limited release of calcium) only allows the formation of these phases, where the Ca/P ratio is between 1 and 1.5 (Table 4). In contrast, release of calcium is enhanced for the mesostructured B75-F127 glass thanks to its bulk reactivity. The precipitation of an apatitic phase (Ca/P = 1.67) is then possible. This assumption is confirmed by the increased stability of the Ca–P phase for the B75-F127 glass demonstrated by chemical mapping (Fig. 4) and evolutions of Ca/P atomic ratios (Fig. 12). Moreover for the B75-F127 glass, the relatively high Ca/P ratio (compared to apatite) between 12 hours and 2 days could be explained by the presence of amorphous or crystallized phases rich in calcium but phosphorus-free,[30] such as calcium oxide CaO, portlandite $Ca(OH)_2$ or calcium carbonate $CaCO_3$. The formation of these phases may be explained by the combination of a massive and rapid release of calcium in the biological medium with a limited source of available phosphorus, which prevent Ca–P phases formation.

The problem developed above for binary glasses does not occur for ternary glasses, because they initially contain phosphorus. Both curves (conventional and mesostructured B67.5) present a similar shape: an exponential decay to a value close to 2.3. This ratio, which is higher than 1.67 (hydroxyapatite), can be due to calcium-rich phases as seen previously.

4.2. Surface *versus* volume precipitation

From the PIXE-RBS mapping obtained, it is clear that Ca–P phases appear within the grains for mesostructured glasses and only at the periphery for the conventional sol–gel glasses.

The first requisite for a bulk precipitation is a high interconnection of pores, in order to facilitate the diffusion of the chemical elements (calcium, phosphorus) involved in the biomineralization process. While mesostructured glasses provide this ideal interconnection, conventional sol–gel glasses do not. Indeed, although the sol–gel naturally generates mesopores, the latter are quite randomly distributed and poorly connected, as evidenced by differences of specific surfaces, which are more than four times higher for materials synthesized using a surfactant (Table 2).

The pore size might also influence the formation of Ca–P phases (particularly hydroxyapatite). Deng *et al.*[31] investigated the effect of pore size on the growth of hydroxyapatite (HA) from mesoporous CaO–SiO_2 substrates. In this work the heterogeneous nucleation of hydroxyapatite is theoretically studied and particularly the critical nuclei size r^*. For low values of r, the nucleus is thermodynamically unstable and dissolved. For larger values of r, the nucleus is thermodynamically stable and persists over time. Nucleation of hydroxyapatite in pores with diameter smaller than $2r^*$ is consequently not allowed because the nuclei are not thermodynamically stable. The calculated range is 0.8 nm < $2r^*$ < 8 nm. This critical radius is consistent with pore diameters of our mesostructured glasses ($2r$ equals to 8.6 and 7.8 for B75-F127 and B67.5-F127 respectively) and could explain why hydroxyapatite and more generally calcium phosphate phases could be formed within the grains of our materials. Moreover Yan *et al.* concluded that small pore size (1.9 nm in their study) could slow down the growth of hydroxyapatite. Indeed, when it occurs, the nucleation stage could easily block small pores and then inhibit the diffusion of Ca^{2+} and HPO_4^{2-} ions which are required to form hydroxyapatite. With this respect, our materials seem to gather all prerequisites for easy CaP formation making them valuable materials for the targeted applications.

5. Conclusions

Three chronological reactions take place during the immersion of SiO_2–CaO and SiO_2–CaO–P_2O_5 glasses in DMEM: calcium release, dissolution of the silica network and precipitation of Ca–P rich phases. A key result of our study is the demonstration that ion beam techniques are powerful to study the effect of mesostructuration over the biomineralization process in sol–gel derived glasses. Indeed, thanks to the use of PIXE-RBS techniques the bulk reactivity of mesostructured glasses is clearly highlighted. This bulk reactivity is a major advantage over conventional glasses, for which the first steps of biomineralization are limited to the outer surface of the material. Two conditions are necessary to allow this bulk reactivity: a high interconnection of pores and pore diameters larger than the critical size for HA precipitation. These two criteria are fully satisfied by our mesostructured glasses explaining their peculiar behavior. Such demonstrated reactivity of mesostructured glasses throughout the material and not only on the outer surface makes them promising materials for bone substitution and combined drug delivery applications.

References

1 S. Myungkoo, L. Ho-Jin, P. Jin-Young, U. H. Lee, K. Young-Uk and K. Deug Joong, *ChemPhysChem*, 2008, **9**, 1402–1408.
2 A. Rámila, B. Muñoz, J. Pérez-Pariente and M. Vallet-Regí, *J. Sol-Gel Sci. Technol.*, 2003, **26**, 1199–1202.
3 C. Charnay, S. Bégu, C. Tourné-Péteilh, L. Nicole, D. A. Lerner and J.-M. Devoisselle, *Eur. J. Pharm. Biopharm.*, 2004, **57**, 533–540.
4 L. L. Hench, *J. Am. Ceram. Soc.*, 1998, **81**, 1705–1728.
5 X. Yan, C. Yu, X. Zhou, J. Tang and D. Zhao, *Angew. Chem., Int. Ed.*, 2004, **43**, 5980–5984.
6 A. Lopez-Noriega, D. Arcos, I. Izquierdo-Barba, Y. Sakamoto, O. Terasaki and M. Vallet-Regi, *Chem. Mater.*, 2006, **18**, 3137–3144.
7 A. J. Salinas, S. Shruti, G. Malavasi, L. Menabue and M. Vallet-Regí, *Acta Biomater.*, 2011, **7**(9), 3452–3458.
8 L. Zhao, X. Yan, X. Zhou, L. Zhou, H. Wang, H. Tang and C. Yu, *Microporous Mesoporous Mater.*, 2008, **109**, 210–215.
9 X. Yan, G. Wei, L. Zhao, J. Yi, H. Deng, L. Wang, G. Lu and C. Yu, *Microporous Mesoporous Mater.*, 2010, **132**, 282–289.
10 X. Yan, X. Huang, C. Yu, H. Deng, Y. Wang, Z. Zhang, S. Qiao, G. Lu and D. Zhao, *Biomaterials*, 2006, **27**, 3396–3403.
11 M. Mozafari, F. Moztarzadeh and M. Tahriri, *J. Non-Cryst. Solids*, 2010, **356**, 1470–1478.
12 M. Vallet-Regi, *Dalton Trans.*, 2006, 5211–5220.

13 C. J. Brinker, Y. F. Lu, A. Sellinger and H. Y. Fan, *Adv. Mater.*, 1999, **11**, 579.
14 J. T. Y. Lee, Y. Leng, K. L. Chow, F. Ren, X. Ge, K. Wang and X. Lu, *Acta Biomater.*, 2011, **7**, 2615–2622.
15 S. Mandel and A. C. Tas, *Mater. Sci. Eng., C*, 2010, **30**, 245–254.
16 D. C. Clupper, J. E. Gough, M. M. Hall, A. G. Clare, W. C. LaCourse and L. L. Hench, *J. Biomed. Mater. Res.*, 2003, **67**, 285–294.
17 T. J. Webster and J. U. Ejiofor, *Biomaterials*, 2004, **25**, 4731–4739.
18 J. E. Gough, I. Notingher and L. L. Hench, *J. Biomed. Mater. Res.*, 2004, **68**, 640–650.
19 J. L. Ong, D. R. Villarreal, R. Cavin and K. Ma, *J. Mater. Sci.: Mater. Med.*, 2001, **12**, 491–495.
20 P. Kundu, T. Waghode, D. Bahadur and D. Datta, *Med. Biol. Eng. Comput.*, 1998, **36**, 654–658.
21 A. Rámila and M. Vallet-Regí, *Biomaterials*, 2001, **22**, 2301–2306.
22 J. Lao, J.-M. Nedelec, P. Moretto and E. Jallot, *Nucl. Instrum. Methods Phys. Res., Sect. B*, 2006, **245**, 511–518.
23 S. Incerti, C. Habchi, P. Moretto, J. Olivier and H. Seznec, *Nucl. Instrum. Methods Phys. Res., Sect. B*, 2006, **249**, 738–742.
24 S. Incerti, Q. Zhang, F. Andersson, P. Moretto, G. W. Grime, M. J. Merchant, D. T. Nguyen, C. Habchi, T. Pouthier and H. Seznec, *Nucl. Instrum. Methods Phys. Res., Sect. B*, 2007, **260**, 20–27.
25 W. Xia and J. Chang, *J. Controlled Release*, 2006, **110**, 522–530.
26 H. S. Yun, S. E. Kim and Y. T. Hyun, *Solid State Sci.*, 2008, **10**, 1083–1092.
27 J. Lao, J. M. Nedelec, P. Moretto and E. Jallot, *Surf. Interface Anal.*, 2008, **40**, 162–166.
28 J. Lao, J. M. Nedelec, P. Moretto and E. Jallot, *Nucl. Instrum. Methods Phys. Res., Sect. B*, 2008, **266**, 2412–2417.
29 X. Lu and Y. Leng, *Biomaterials*, 2005, **26**, 1097–1108.
30 M. Bini, S. Grandi, D. Capsoni, P. Mustarelli, E. Saino and L. Visai, *J. Phys. Chem. C*, 2009, **113**, 8821–8828.
31 Y. Deng, X. Li and Q. Li, *Ind. Eng. Chem. Res.*, 2009, **48**, 8829–8836.